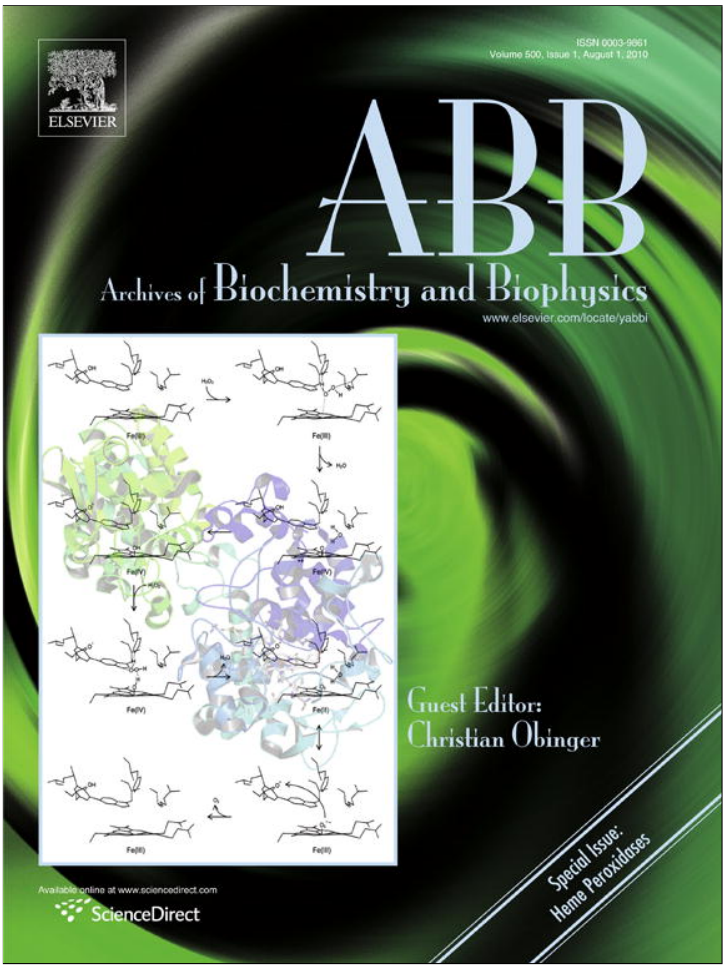

Archives of Biochemistry and Biophysics 500 (2010) 37–44

Contents lists available at ScienceDirect

Archives of Biochemistry and Biophysics

journal homepage: www.elsevier.com/locate/yabbi

Review

The dynamic role of distal side residues in heme hydroperoxidase catalysis. Interplay between X-ray crystallography and *ab initio* MD simulations

Pietro Vidossich [a,b], Mercedes Alfonso-Prieto [a,b], Xavi Carpena [c], Ignacio Fita [d], Peter C. Loewen [e], Carme Rovira [a,b,f,*]

[a] *Laboratori de Simulació Computacional i Modelització (CoSMoLab), Parc Científic de Barcelona, Josep Samitier 1-5, 08028 Barcelona, Spain*
[b] *Institut de Química Teòrica i Computacional (IQTCUB), Spain*
[c] *Institute of Research in Biomedicine (IRB-Barcelona) and Institut Químic de Sarrià (IQS), Parc Científic de Barcelona, Baldiri Reixac 10-12, 08028 Barcelona, Spain*
[d] *Institute of Research in Biomedicine (IRB-Barcelona) and Institut de Biologia Molecular (IBMB-CSIC), Parc Científic de Barcelona, Baldiri Reixac 10-12, 08028 Barcelona, Spain*
[e] *Department of Microbiology, University of Manitoba, Winnipeg, MB, Canada R3T 2N2*
[f] *Institució Catalana de Recerca i Estudis Avançats (ICREA), Passeig Lluís Companys, 23, 08018 Barcelona, Spain*

ARTICLE INFO

Article history:
Received 24 February 2010
and in revised form 27 April 2010
Available online 4 May 2010

Keywords:
Ab initio molecular dynamics
Density functional theory
Hydroperoxidases
Catalases
Peroxidases
Enzyme catalysis

ABSTRACT

The enzymatic cycle of hydroperoxidases involves the resting Fe(III) state of the enzyme and the high-valent iron intermediates Compound I and Compound II. These states might be characterized by X-ray crystallography and the transition pathways between each state can be investigated using atomistic simulations. Here we review our recent work in the modeling of two key steps of the enzymatic reaction of hydroperoxidases: the formation of Cpd I in peroxidase and the reduction of Cpd I in catalase. It will be shown that small conformational motions of distal side residues (His in peroxidases and His/Asn in catalases), not, or only partially, revealed by the available X-ray structures, play an important role in the catalytic processes examined.

Introduction

It is nowadays well accepted that proteins should not be pictured as static objects, but rather as dynamic systems [1,2]. It is also recognized that there must be a detailed balance, encoded in the amino acids sequence, between stability and flexibility since protein function generally requires some degree of conformational motion [1]. These requirements are unified under the concept of the free energy landscape (FEL)[1], i.e. the free energy as a function of the atomic coordinates of the system [3]. Its knowledge would tell us about the stable states of the system (wells on the FEL), their population (Boltzmann probabilities) and the paths by which they are interconnected (likely overcoming energy barriers), guiding us towards an understanding of protein folding [4,5], signal transmission [6], ligand binding [7], transportation [8] and chemical catalysis [9]. It is thus not surprising that much effort has been and is dedicated to the development of experimental and computational techniques for its characterization. Yet, even for the most studied system, large parts of the surface are still unknown. Much of today's understanding of the topology of a protein FEL has been modeled on extensive studies of the heme protein myoglobin [3,10]. X-ray crystallography, spectroscopy and molecular dynamics simulations contributed to picture the FEL as a rugged surface organized in a hierarchy of tiers depending on the magnitude of the barriers that separate the wells. Higher tiers comprise few functional states separated one another by large barriers, such that transitions from one to another are rare events, with each one comprising a large number of conformational substates separated by smaller energy barriers [3,11]. This classification turns out also to be an operational one, as the magnitude of the barriers determine the time scale by which (sub)states interconvert and thus dictate the choice of the technique to be used to investigate transitions [1].

In the context of enzymatic catalysis, the mechanisms by which protein fluctuations are coupled to the reactive events are still under debate [12], but it is becoming increasingly evident that

* Corresponding author at: Laboratori de Simulació Computacional i Modelització (CoSMoLab), Parc Científic de Barcelona, Josep Samitier 1-5, 08028 Barcelona, Spain.
E-mail address: crovira@pcb.ub.es (C. Rovira).

[1] Abbreviations used: FEL, free energy landscape; MD, molecular dynamics; QM/MM, quantum mechanics/molecular mechanics; Cpd I, Compound I; Cpd II, Compound II; Cpd I*, Compound I*; HRP, horseradish peroxidase; KatG, catalase-peroxidase; CcP, cytochrome c peroxidase; APX, ascorbate peroxidase; VP, versatile peroxidase; MnP, manganese peroxidase; BGP, barley grain peroxidase; HPC, *Helicobacter pylori* catalase; HEC, human erythrocyte catalase; HPII, *Escherichia coli* hydroperoxidase II; MLC, *Micrococcus lysodeikticus* catalase; CatF, *Pseudomonas syringae* catalase F; PMC, *Proteus mirabilis* catalase; NCC-1, *Neurospora crassa* catalase-1; VSC, *Vibrio salmonicida* catalase.

0003-9861/$ - see front matter © 2010 Elsevier Inc. All rights reserved.
doi:10.1016/j.abb.2010.04.021

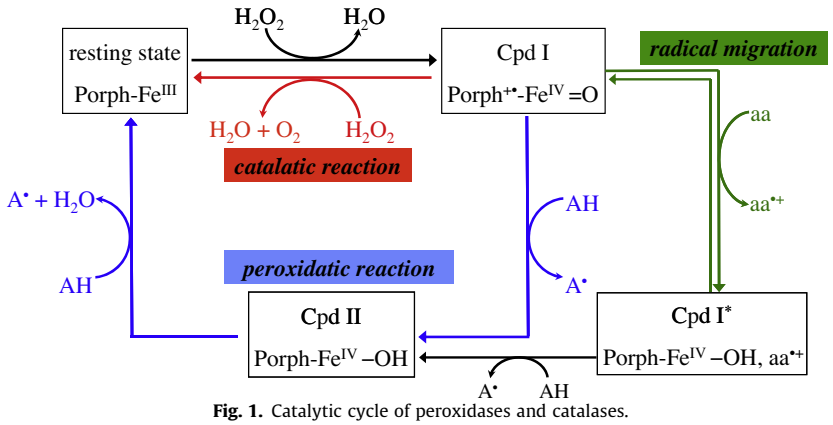

Fig. 1. Catalytic cycle of peroxidases and catalases.

characteristic motions of the protein, present in the native state, preferentially follow the pathways that create the configuration optimum for catalysis [9]. Some of these pathways can be analyzed by classical molecular dynamics (MD) simulations [11], whereas subtle motions of active site residues, often coupled to electronic rearrangements, can be captured by *ab initio* MD simulations [13].

Here we are interested in the characterization of local conformational changes which are relevant for catalysis by hydroperoxidases [14]. The enzymatic cycle of hydroperoxidases involves at least three stable states (Fig. 1): the resting state (Porph-Fe^{III}) and the high-valent intermediates, Compound I (Cpd I) and Compound II (Cpd II). Cpd I is normally an oxoferryl porphyrin cation radical (Porph$^{+\cdot}$-Fe^{IV}=O) although, in some hydroperoxidases, the second oxidizing equivalent may reside on a protein residue (Porph-Fe^{IV}=O, $aa^{+\cdot}$, named Compound I*, Cpd I*) [15]. In contrast, Compound II is an oxo/hydroxoferryl species (Porph-Fe^{IV}=O/Porph-Fe^{IV}–OH) and lacks the porphyrin (or protein) radical. These states correspond to deep wells of the competent FEL and, in some cases, have been characterized by X-ray crystallography (see e.g. Ref. [16]). Unfortunately, description of the transition pathways between them at atomic resolution is out of experimental reach. However, the corresponding transitions can be modeled using MD-based techniques based on hybrid quantum mechanics/molecular mechanics (QM/MM) interaction potentials.

In this work, we review our recent *ab initio* modeling of two key steps of the enzymatic cycle of hydroperoxidases: the formation of Cpd I in horseradish peroxidase (HRP) [17,18] and the reduction of Cpd I in *Helicobacter pylori* catalase (HPC) [19]. HRP is among the most studied peroxidase enzymes [14] and HPC is one of the few catalases for which a high resolution Cpd I structure is available [20]. Both HRP and HPC share the same type of heme cofactor (heme b or protoporphyrin IX). We will show how conformational changes of distal side residues are required for efficient catalysis. Furthermore, we will take a step backwards analyzing high resolution structures of the different states of hydroperoxidases trying to identify structural features that could suggest the conformational changes observed in the atomistic simulations. This exercise will lead us to conclude that the interplay between X-ray crystallography, to characterize stable states on FEL, and atomistic modeling, to investigate transition paths, will continue to provide valuable insight into the molecular details of enzymatic catalysis.

Peroxidases

The active site of peroxidases (Fig. 2) consists of a heme group with an axially coordinated histidine (His170 in HRP), which in most peroxidases is hydrogen bonded to an aspartate residue (Asp247). On the heme distal side, there are one histidine and one arginine residue (His42 and Arg38, respectively) [14,21].

Peroxidase Compound I forms from the resting Fe^{III} state of the enzyme by reaction with hydrogen peroxide (Fig. 1), although in vitro other oxidants may be used. Several clues about the catalytic mechanism are provided by experimental investigations. It was early shown by kinetic studies that formation of Compound I involves at least one reversible intermediate [22,23]. In a seminal work, Poulos and Kraut [24], on the basis of their studies on the crystal structure of CcP [25], proposed a mechanism (Scheme 1) that was capable of rationalizing mutagenesis experiments showing a five orders of magnitude decrease in the rate of formation of Cpd I for the CcP-His52Leu mutant [26] and two orders reduction for Arg48Leu [32]. Similar results were obtained from the corresponding HRP mutants [21,26,27]. In the Poulos–Kraut mechanism, the histidine residue on the distal side of the heme (His42) deprotonates H_2O_2, leading to the formation of a ferric hydroperoxide intermediate (Por-Fe^{III}–OOH) that was later called Compound 0 (Cpd 0). Based on considerations of the acidities of the species involved, Jones and Dunford [28] argued that such proton transfer (from H_2O_2 to His42) should take place once the peroxide is bound to the iron.

Atomistic modeling

The energy barrier for the direct proton abstraction by the distal His in horseradish peroxidase (Scheme 1), computed by QM/MM calculations [29], was found to be very high (~20 kcal/mol). This high deprotonation barrier, attributed to the long distance between His42 and the proximal proton of the Fe–H_2O_2 complex ($N_{\varepsilon}\cdots H_a \sim 4$ Å, see Scheme 1), indicates that something is missing in the atomistic model. This mechanistic puzzle was solved by analyzing the magnitude of protein fluctuations [17]. It was shown by classical molecular dynamics studies that the active site of HRP is rather stiff [17,30] and His42 does not approach H_a closely. This is consistent with the (relatively low) B factors of the HRP distal residues (Table 1) in the native state and Cpd I. However, analysis of the dynamics of the water molecules in the heme pocket pointed out an apparently simple detail with potential consequences for catalysis: conformations in which a water molecule comes to bridge H_a and His42 (Scheme 2) often occur [18]. This suggests that a relay mechanism via the bridging water molecule could be operative in HRP. Indeed, QM/MM calculations in the presence of such a bridging water molecule [17] showed that the energy barrier for H_2O_2 deprotonation is drastically reduced (from ~20 to ~5 kcal/mol) compared with the direct transfer.

The complete mechanism for Cpd I formation in HRP, obtained by combining classical and *ab initio* (QM/MM) MD simulations, is shown in Fig. 3. Water-mediated proton transfer from H_2O_2 to His42 leads to Cpd 0, in which His42(H^+) hydrogen bonds with the catalytic water molecule(s). As revealed by *ab initio* MD simulations, His42(H^+) easily exchanges hydrogen bond partner to O_b of the

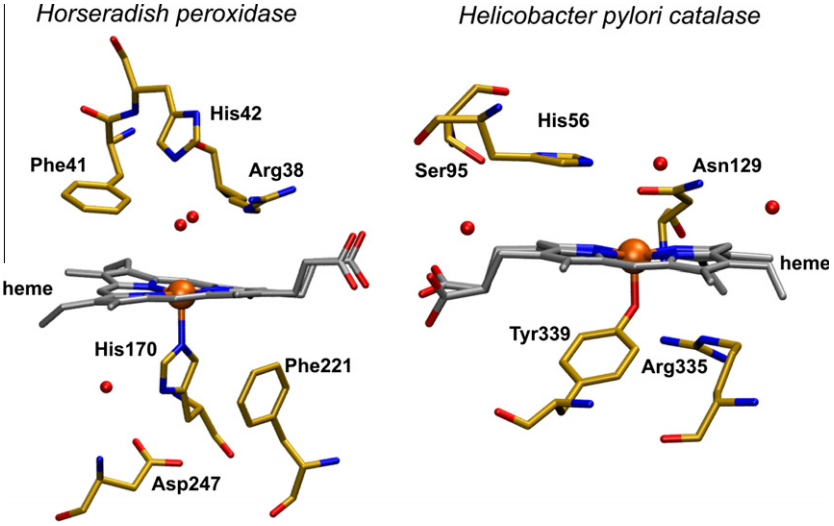

Fig. 2. Active site of HRP and HPC.

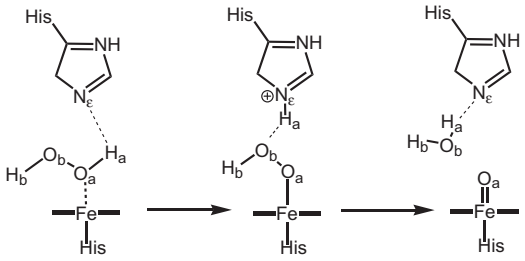

Scheme 1. The Poulos–Kraut mechanism.

peroxide, displacing the water molecule. Because this interchange was observed more than once in room temperature (300 K) *ab initio* MD simulations, we assume the underlying barrier to be small. At the same time, Arg38 undergoes small fluctuations (Fe···N_ε(Arg) = 4.44 ± 0.21 Å). Once His42–H^+ interacts with O_b of the peroxide, it delivers the proton to it [29], leading to the concerted heterolytic breakage of the peroxide O_a–O_b bond with formation of Cpd I and a water molecule. This step displays the highest barrier along the whole process (~12.5–15 kcal/mol, depending on initial conformation). The overall mechanism (Fig. 3) involves the same intermediate put forward by Poulos and Kraut (Scheme 1), but differs from it in the first step of the process, i.e. formation of Cpd 0, which takes place with the assistance of one water molecule. Furthermore, the conversion from Cpd 0 to Cpd I requires a small amplitude motion of His42 (~1 Å) to switch hydrogen bonding partner from a water molecule to the peroxide (Fig. 3). A similar mechanism, involving two water molecules, has been recently proposed for Cpd I formation upon reaction of KatG with peracetic acid [31]. Catalases, with the distal His in a different orientation from peroxidases (Fig. 2), are not expected to need assistance of a water molecule to form Cpd I.

Analysis of X-ray structures

We will now analyze high resolution structures of the native and Cpd I forms of peroxidases trying to pinpoint clues which could suggest the motion of the distal His observed in the atomistic modeling. Only structures at resolution higher than 2.2 Å have been considered and only one structure for each type of peroxidase is listed (the highest resolution one). Since it is not possible to distinguish among the intermediates of the catalytic cycle of hydroperoxidases (Cpds I, I* and II), which only differ in one electron or its location within the protein, on the basis of structure alone (see e.g. Refs. [20,32,33]), we have decided to include in the analysis also putative Cpd I* and II species and label high-valent states with the superindex "ox".

Table 1
Peroxidase distal structure and average B factors (B_f).

Peroxidase	Class	PDB ID	Resol. (Å)	Fe···His[a] (Å)	Fe···Arg[b] (Å)	Fe···Phe[c] (Å)	Fe···Trp[c] (Å)	Fe···O[d] (Å)	Relative B_f[e] (Heme/His/Arg/Phe/Trp)
KatG	I	1MWV	1.7	5.57	6.49	–	4.45	2.55	0.68/0.80/0.73/–/0.81
CcP	I	1ZBY	1.2	5.45	4.19/5.90	–	4.07	2.33	0.66/0.77/0.77/–/0.70
APX	I	1OAG	1.75	5.46	6.09	–	3.98	1.87	0.79/0.87/0.95/–/0.82
VP	II	3FMU	1.04	5.61	5.75	5.15	–	2.73	0.62/0.65/0.78/0.74/–
MnP	II	1YYD	1.45	5.51	4.93/6.19	5.01	–	2.32	0.74/0.61/0.79/0.76/–
HRP	III	1ATJ	2.15	5.99	4.61	4.53	–	3.20	0.67/0.43/0.44/0.44/–
BGP	III	1BGP	1.9	8.21	5.44	3.83	–	5.75	0.54/0.75/0.59/0.54/–
$KatG^{ox}$	I	2B2R	1.9[f]	5.49	6.32	–	5.49	2.09	0.68/0.72/0.65/–/0.74
	I	2B2S	2.0	5.55	6.32	–	5.55	1.88	0.77/0.76/0.73/–/0.78
CcP^{ox}	I	1ZBZ	1.29	5.43	4.03	–	3.90	1.87	0.68/0.75/0.73/–/0.67
HRP^{ox}	III	1HCH	1.57	5.65	4.17	4.43	–	1.70	0.60/0.60/0.63/0.59/–

[a] Distance from the Fe atom to the N_ε of the distal His.
[b] Distance from the Fe atom to the N_ε of the distal Arg.
[c] Distance from the Fe atom to the closest C/N atom of the distal Phe/Trp.
[d] Closest oxygen to the Fe regardless of whether it belongs to a ligated/unligated water or it is the oxoferryl/hydroxoferryl oxygen of Cpd I/Cpd II.
[e] Average B factor of the given residue, relative to the average protein B factor.
[f] Values at pH 5.6 and 7.5.

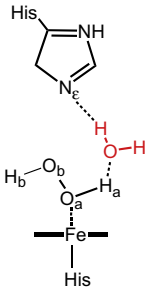

Scheme 2.

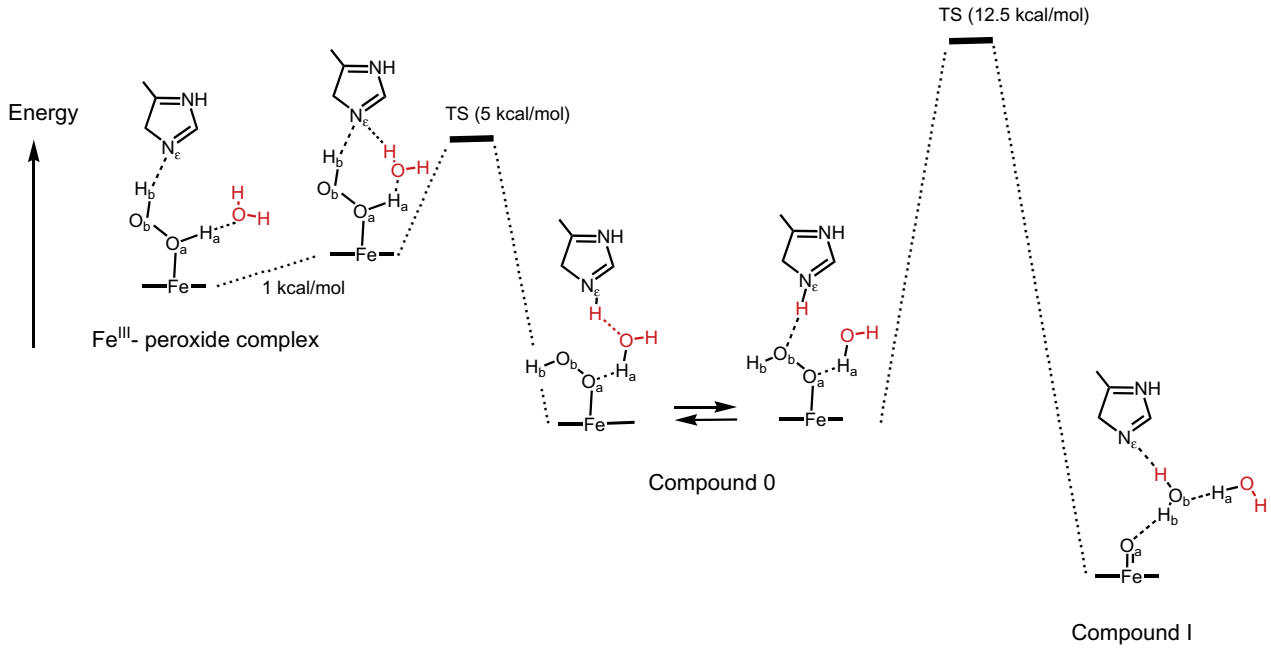

Fig. 3. Mechanism of Cpd I formation in horseradish peroxidase.

Table 1 lists some structural parameters defining the position of distal side residues relative to the iron and the average B factors reported in the original works. All peroxidases display a similar distal side structure. The distal His is ~5.5 Å from the iron atom, independently of the active site oxidation state (the anomalously far-away position of the His in BGP is due to a dramatic structural rearrangement of one loop region at neutral pH, which precludes Cpd I formation thus inactivating the enzyme [34]). On the contrary, the position of the distal Arg shows appreciable differences (Fe···Arg distances ~4.1–6.19) and, in some cases (native CcP and MnP) adopts two orientations. Such conformational freedom could be related to its involvement in substrate binding in the later steps of the peroxidatic cycle. As for B factors, those of distal residues are equal or slightly above those of the heme group. Our analysis thus indicates that the distal His has similar orientation with respect to the heme group in the resting state and in Cpd I and displays positional fluctuations of the same order of the neighboring residues. Therefore, no hints of a conformational change could be detected in the X-ray data. However, to conclude this section, we want to give credit to Poulos and Kraut who predicted the acid/base role of the distal His on the basis of the X-ray structure of CcP.

Catalases

The active site of catalases (Fig. 2) consist of a heme group with an axially coordinated tyrosine (Tyr339 in HPC), which is hydrogen bonded to an arginine residue (Arg335). On the heme distal side, there are one histidine and one asparagine residue (His56 and Asn129, respectively).

In the catalatic reaction, Cpd I ($Por^{\bullet+}$-Fe^{IV}=O) is reduced back to the resting state by a second molecule of hydrogen peroxide (Fig. 1), which serves as a two-electron reductant. Formally, one electron reduces the porphyrin radical, while the other one contributes to the change of oxidation state of the iron atom (from Fe^{IV} to Fe^{III}). The transfer of two electrons from H_2O_2 is associated with the transfer of two protons to the oxoferryl oxygen, forming a water molecule. Since the determination of the X-ray structure of a catalase, it was proposed that the reaction should proceed stepwise [35]. In particular, Fita and Rossmann proposed that the distal His would act as an acid base catalyst facilitating the transfer of a proton from the peroxide to the oxoferryl unit (see Scheme 3). Because of this, an H^+/H^- scheme was assumed, in which H^- is transferred directly to the oxoferryl unit and the transfer of H^+ is mediated by the distal His.

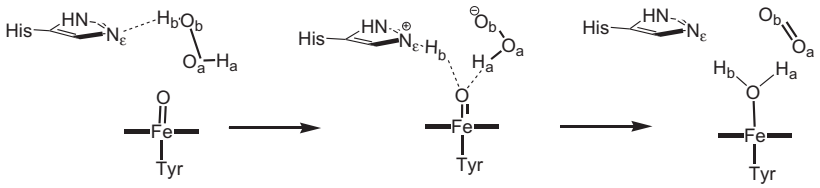

Scheme 3. The Fita-Rossmann mechanism

Atomistic modeling

Recent modeling of the catalase reaction in catalases from *Helicobacter pylori* and *Penicillium vitale* (HPC and PVC) by means of QM/MM metadynamics simulations showed that the reaction proceeds via the Fita–Rossmann mechanism [19]. Nevertheless, the overall process does not proceed by a proton and hydride transfer as has often been assumed [35], but rather by sequential two one electron transfers in the form of a hydrogen atom transfer and a concerted proton and electron transfer. The first step consists of a facile hydrogen transfer from H_2O_2 to Cpd I (Fig. 4) leading to Cpd II + $HO_2^{\cdot}$. The small energy cost for this hydrogen atom transfer was attributed to the short interatomic distances between donor and acceptor oxygen atoms. This can be attained in the active site of catalases thanks to the particular orientation of His56, with its imidazole side chain being almost parallel to the heme (Fig. 2) holding H_2O_2 in place for catalysis. In fact, an *in silico* His56Gly mutant (HPC numbering) exhibits a much higher energy barrier and becomes the rate-limiting step [19].

Conversion of Cpd II + $HO_2^{\cdot}$ to the resting state of the enzyme is a complex process that can take place via two competing pathways (Fig. 4). In the first pathway (A), a proton is transferred from $HO_2^{\cdot}$ to His56, which then changes conformation [the Fe···N_ε(His) distance decreases by ~0.8 Å] to facilitate breaking of the H-bond with superoxide and formation of a new one with the oxoferryl oxygen. This conformational change of His56 represents the highest energy demanding step along pathway A. The new conformation of His56 allows the facile transfer of the H_b proton (Fig. 4) which occurs together with the passage of an electron from superoxide to the oxoferryl.

A competing pathway (B) was found in HPC for the conversion of Cpd II + $HO_2^{\cdot}$ to the resting state of the enzyme. In pathway B, a flip of the peroxyl radical reorients its proton towards the oxoferryl oxygen, facilitating a direct hydrogen atom transfer (Fig. 4). Our analysis indicates the basicity of His56 and the distal site cavity to be important factors governing the relative probability of the two pathways.

Fig. 5 shows the detailed atomic and electronic spin density changes during the reaction in HPC. The two alternative pathways (A and B) are clearly differentiated in the computed FEL as a function of two reaction coordinates (central panel). The FEL is rather rugged, with several local minima of different well depth. The rotational motion of His56 becomes evident when following the atomic changes along each pathway. Although subtle, the rotation of His causes the transient breaking up of its hydrogen bond with the side chain of Ser95 (His56–N_δH···OH–Ser95). Another interesting feature of the mechanism is the rotation of the Asn129 side chain towards the main channel [the Fe···N_δ(Asn) distance increases by ~0.6 Å], facilitating the escape of the oxygen molecule released in the reaction.

Analysis of X-ray structures

Table 2 lists some parameters defining the position of the catalase distal side residues (His and Asn) along with their average B factors (B_f). Structures at resolution lower than 2.2 Å have not been considered and only one structure for each type of catalase is listed. As for peroxidases, we label the structures of the reaction intermediates with the superindex "ox", without specifying whether it is Cpd I, II or I*. Unlike peroxidases, the essential distal His of catalases adopts an almost parallel orientation with the heme (Fig. 2), with its N_ε separated by 4.6–4.8 Å from the iron atom in the native state, becoming slightly closer (by ~0.2–0.3 Å) in the oxidized state. Thus, contrary to peroxidases, in which the distal His was observed in the same orientation in the resting and Cpd I states, in catalases the distal His adopts slightly different orientations in the resting and Cpd I forms. Since X-ray crystallography reveals stable structures corresponding to minima on the FEL, this indicates that the distal His probably undergoes a conformational change, though small, during the transition from Cpd I to the resting state, as found in the *ab initio* simulations. However, since the structure of Cpd I was not solved under catalytic conditions, rather it was prepared by reaction with a suitable peracid, we cannot conclude that the inferred conformational change is involved in the chemical step.

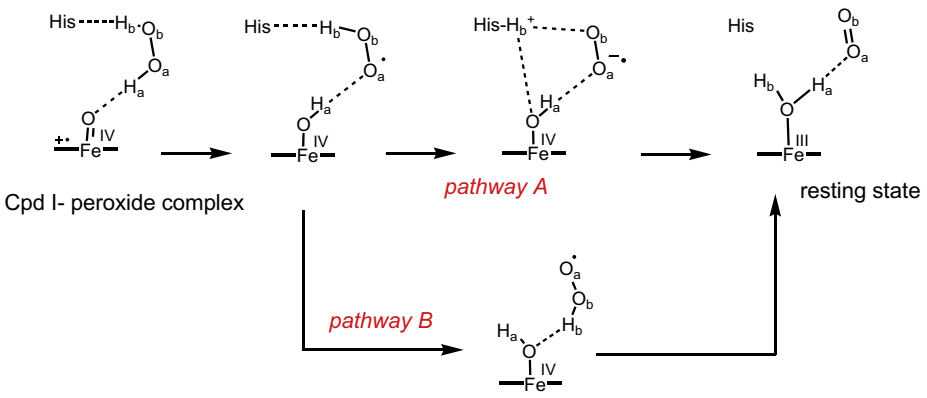

Fig. 4. Mechanism of Cpd I reduction in catalase.

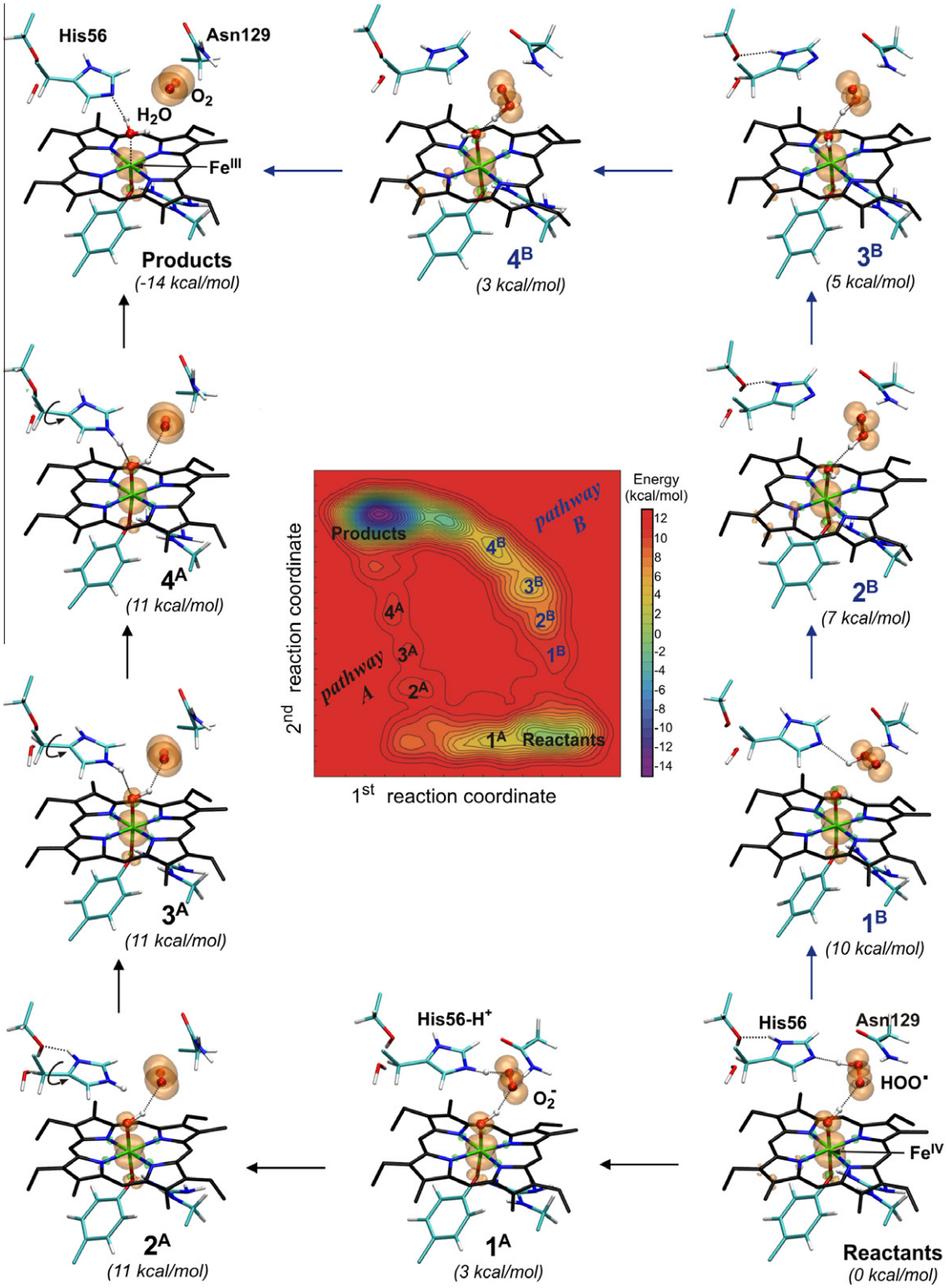

Fig. 5. Electronic/structural rearrangement during the conversion of Cpd II—OOH· to the resting state in HPC. Contour lines are spaced by 1 kcal/mol. The energy of the different points along the pathway, relative to the reactants, is given below each structure label.

A further point of interest concerns the distal Asn which does not exhibit any significant conformational difference between the resting and oxidized states. It is intriguing, however, that the carbonyl group of the distal Asn, unlike other Asn residues in the protein, is not involved in any hydrogen bond interaction with other protein residues which would restrain its conformational flexibility. This could indicate a functional role for this residue, possibly related to entrance/release of reactants/products, as observed in the atomistic modeling. Even though the distal Asn is not an essential residue in catalases, its mutation decreases the catalase activity by 80% [15,36].

Table 2
Catalase distal structure and average B factors (B_f).

Catalase	PDB ID	Resol. (Å)	Fe···His[a] (Å)	Fe···Asn[b] (Å)	His···Asn (Å)	His···Ser[c] (Å)	Fe···O[d] (Å)	Relative B_f[e] (Heme/His/Asn)
HEC	1DGF	1.5	4.66	6.24	3.99	2.84	4.11	0.67/0.71/0.81
HPII	1GGE	1.9	4.66	6.79	3.98	2.81	3.01	0.61/0.44/0.53
MLC	1GWE	0.88	4.60	6.26	3.81	2.76	2.31	0.62/0.63/0.65
CatF	1M7S	1.8	4.67	6.72	4.19	2.82	2.35	0.67/0.60/1.01
PMC	1M85	2.0	4.83	6.45	4.04	2.83	3.46	0.68/0.68/0.76
HPC	1QWL	1.6	4.67	6.36	3.97	2.78	2.71	0.75/0.62/0.77
NCC-1	1SY7	1.75	4.89	6.74	4.08	2.72	4.64	0.58/0.60/0.73
VSC	2ISA	1.97	4.63	6.48	4.00	2.88	4.81	0.76/0.59/0.73
MLC^{ox}	1GWF	1.96	4.48	6.26	3.97	2.66	1.86	0.83/0.72/0.78
HPC^{ox}	2IQF	1.86	4.53	6.31	4.16	2.85	1.83	0.77/0.63/0.86
PVC^{ox}	2IUF	1.71	4.41	6.64	4.04	2.79	1.72	0.83/0.76/0.84

[a] Distance from the Fe atom to the N_ε of the distal His.
[b] Distance from the Fe atom to the N_δ of the distal Asn.
[c] Distance from the distal His N_δ atom to the hydroxyl oxygen of its interacting Ser.
[d] Closest oxygen to the Fe regardless of whether it belongs to a ligated/unligated water or it is the oxoferryl/hydroxoferryl oxygen of Cpd I/Cpd II.
[e] Average B factor of the given residue, relative to the average protein B factor.

Conclusions

The interplay between X-ray crystallography and molecular dynamics (MD) simulations became evident very soon after the introduction of the latter technique, with a textbook example being the study of myoglobin [37–39]. X-ray crystallography generally provides atomic resolution structures of the stable states of the system. Different states may be accessed changing the conditions of the experiment (e.g. pH, presence of ligands). Under specific conditions, it has been possible to reveal reactive intermediates [16,40] and follow the evolution of the enzymatic reaction [41] or ligand binding [42]. MD simulations move from X-ray structures to provide a picture of the system at nearly physiological conditions, i.e. room temperature and solution [11]. In the ideal case, MD would provide a detailed picture of not only the stable states, but also the atomic rearrangements which take place during transitions. Unfortunately, MD experiences limitations deriving from the accuracy of the potential energy functions used and the time scale accessible by the simulation. The accuracy limit may be partially overcome by the use of *ab initio* MD, in which the interatomic forces are computed from electronic structure methods (e.g. Density Functional Theory). This limits even further the time scale accessible by the simulations (tens of picoseconds) and, when direct dynamics do not reveal the transition of interest within the time span, special simulation techniques (e.g. metadynamics [43]) need to be used.

Here we have shown how the conformational change of the distal His in hydroperoxidases facilitates proton transfer from the substrate to the heme cofactor. In peroxidases, the simulation shows that His42 rotates around C_β–C_γ to change hydrogen bond partner (from a water oxygen atom to the distal peroxide oxygen) [17]. In catalases, a conformational change of the $HisH^+$ leads to the formation of a hydrogen bond with the hydroxoferryl heme, facilitating proton transfer and the conversion of Cpd I to the resting state of the enzyme [19]. The simulations also capture the motion of the distal Asn to accommodate the oxygen released during catalysis. These subtle motions of active site residues, essential for catalysis, are not, or only partially, evidenced by analysis of the crystal structures, underscoring the need to complement structural studies with *ab initio* MD simulations to obtain a more complete picture of the catalytic process.

Acknowledgments

The authors thank the Spanish Ministry of Science and Innovation (MICINN) (Grant FIS2008-03845) and the Generalitat de Catalunya (Grant 2009SGR-1309) for its financial assistance. P.V. acknowledges a Juan de la Cierva contract from MCINN. We acknowledge the computer support, technical expertise, and assistance provided by the Barcelona Supercomputing Center-Centro Nacional de Supercomputación (BSC-CNS). The work was also supported by a Discovery Grant 9600 from the Natural Sciences and Engineering Research Council (NSERC) of Canada (to PCL) and by the Canada Research Chair Program (to PCL). We are grateful to S. Shaik, E. Derat and G. Fiorin for discussions and collaboration concerning this work.

References

[1] K. Henzler-Wildman, D. Kern, Nature 450 (2007) 964–972.
[2] J.A. McCammon, M. Karplus, Acc. Chem. Res. 16 (1983) 187–193.
[3] H. Frauenfelder, S.G. Sligar, P.G. Wolynes, Science 254 (1991) 1598–1603.
[4] D. Baker, Nature 405 (2000) 39–42.
[5] H.R. Kalbitzer, M. Spoerner, P. Ganser, C. Hozsa, W. Kremer, J. Am. Chem. Soc. 131 (2009) 16714–16719.
[6] R.G. Smock, L.M. Gierasch, Science 324 (2009) 198–203.
[7] G.M. Lee, C.S. Craik, Science 324 (2009) 213–215.
[8] S.Y. Noskov, S. Berneche, B. Roux, Nature 431 (2004) 830–834.
[9] K.A. Henzler-Wildman, V. Thai, M. Lei, M. Ott, M. Wolf-Watz, T. Fenn, E. Pozharski, M.A. Wilson, G.A. Petsko, M. Karplus, C.G. Hubner, D. Kern, Nature 450 (2007) 838–844.
[10] A. Ansari, J. Berendzen, S.F. Bowne, H. Frauenfelder, I.E. Iben, T.B. Sauke, E. Shyamsunder, R.D. Young, Proc. Natl. Acad. Sci. USA 82 (1985) 5000–5004.
[11] M. Karplus, J.A. McCammon, Nat. Struct. Biol. 9 (2002) 646–652.
[12] M.H. Olsson, W.W. Parson, A. Warshel, Chem. Rev. 106 (2006) 1737–1756.
[13] P. Carloni, U. Rothlisberger, M. Parrinello, Acc. Chem. Res. 35 (2002) 455–464.
[14] H.B. Dunford, Heme Peroxidases, John Wiley, New York; Chichester, 1999.
[15] I.F.P. Nichols, P.C. Loewen, in: G.M.A.G. Sykes (Ed.), Advances in Inorganic Chemistry, Academic Press, 2001, pp. 51–106.
[16] G.I. Berglund, G.H. Carlsson, A.T. Smith, H. Szoke, A. Henriksen, J. Hajdu, Nature 417 (2002) 463–468.
[17] E. Derat, S. Shaik, C. Rovira, P. Vidossich, M. Alfonso-Prieto, J. Am. Chem. Soc. 129 (2007) 6346–6347.
[18] P. Vidossich, G. Fiorin, M. Alfonso-Prieto, E. Derat, S. Shaik, C. Rovira, J. Phys. Chem. B 114 (2010) 5161–5169.
[19] M. Alfonso-Prieto, X. Biarnes, P. Vidossich, C. Rovira, J. Am. Chem. Soc. 131 (2009) 11751–11761.
[20] M. Alfonso-Prieto, A. Borovik, X. Carpena, G. Murshudov, W. Melik-Adamyan, I. Fita, C. Rovira, P.C. Loewen, J. Am. Chem. Soc. 129 (2007) 4193–4205.
[21] J.N. RodriguezLopez, A.T. Smith, R.N.F. Thorneley, J. Biol. Chem. 271 (1996) 4023–4030.
[22] H.K. Baek, H.E. Van Wart, Biochemistry 28 (1989) 5714–5719.
[23] P. Jones, H.B. Dunford, J. Theor. Biol. 69 (1977) 457–470.
[24] T.L. Poulos, J. Kraut, J. Biol. Chem. 255 (1980) 8199–8205.
[25] T.L. Poulos, S.T. Freer, R.A. Alden, S.L. Edwards, U. Skogland, K. Takio, B. Eriksson, N. Xuong, T. Yonetani, J. Kraut, J. Biol. Chem. 255 (1980) 575–580.
[26] J.E. Erman, L.B. Vitello, M.A. Miller, A. Shaw, K.A. Brown, J. Kraut, Biochemistry 32 (1993) 9798–9806.
[27] J.N. RodriguezLopez, A.T. Smith, R.N.F. Thorneley, J. Biol. Inorg. Chem. 1 (1996) 136–142.
[28] P. Jones, H.B. Dunford, J. Inorg. Biochem. 99 (2005) 2292–2298.
[29] E. Derat, S. Shaik, J. Phys. Chem. B 110 (2006) 10526–10533.
[30] C. Zazza, A. Amadei, A. Palma, N. Sanna, S. Tatoli, M. Aschi, J. Phys. Chem. B 112 (2008) 3184–3192.

[31] B. Wiseman, J. Colin, A.T. Smith, A. Ivancich, P.C. Loewen, J. Biol. Inorg. Chem. 14 (2009) 801–811.
[32] G.N. Murshudov, A.I. Grebenko, J.A. Brannigan, A.A. Antson, V.V. Barynin, G.G. Dodson, Z. Dauter, K.S. Wilson, W.R. Melik-Adamyan, Acta Crystallogr., Sect. D: Biol. Crystallogr. 58 (2002) 1972–1982.
[33] C.A. Bonagura, B. Bhaskar, H. Shimizu, H. Li, M. Sundaramoorthy, D.E. McRee, D.B. Goodin, T.L. Poulos, Biochemistry 42 (2003) 5600–5608.
[34] A. Henriksen, K.G. Welinder, M. Gajhede, J. Biol. Chem. 273 (1998) 2241–2248.
[35] I. Fita, M.G. Rossmann, J. Mol. Biol. 185 (1985) 21–37.
[36] B. Gao, W.E. Boeglin, A.R. Brash, Arch. Biochem. Biophys. 477 (2008) 285–290.
[37] R. Elber, M. Karplus, Science 235 (1987) 318–321.
[38] M. Meuwly, O.M. Becker, R. Stote, M. Karplus, Biophys. Chem. 98 (2002) 183–207.
[39] C. Rovira, B. Schulze, M. Eichinger, J.D. Evanseck, M. Parrinello, Biophys. J. 81 (2001) 435–445.
[40] I. Schlichting, J. Berendzen, K. Chu, A.M. Stock, S.A. Maves, D.E. Benson, R.M. Sweet, D. Ringe, G.A. Petsko, S.G. Sligar, Science 287 (2000) 1615–1622.
[41] E.G. Kovaleva, J.D. Lipscomb, Science 316 (2007) 453–457.
[42] F. Schotte, M. Lim, T.A. Jackson, A.V. Smirnov, J. Soman, J.S. Olson, G.N. Phillips Jr., M. Wulff, P.A. Anfinrud, Science 300 (2003) 1944–1947.
[43] A. Laio, M. Parrinello, Proc. Natl. Acad. Sci. USA 99 (2002) 12562–12566.